Ultrashort optical waveguide excitations in uniaxial silica fibers: Elastic collision scenarios

Victor K. Kuetche,[1,2,3,4,*] Saliou Youssoufa,[2,3,4,†] and Timoleon C. Kofane[3,4,‡]

[1]*Abdus Salam International Centre for Theoretical Physics (ICTP), Strada Costiera, 11-I-34151 Trieste, Italy*

[2]*National Advanced School of Engineering, University of Yaounde I, P. O. Box 8390, Cameroon*

[3]*Centre d'Excellence en Technologies de l'Information et de la Communication (CETIC), University of Yaounde I, P. O. Box 812, Yaounde, Cameroon*

[4]*Department of Physics, Faculty of Science, University of Yaounde I, P. O. Box 812, Cameroon*

(Received 12 June 2014; revised manuscript received 6 November 2014; published 23 December 2014)

In this work, we investigate the dynamics of an uniaxial silica fiber under the viewpoint of propagation of ultimately ultrashort optical waveguide channels. As a result, we unveil the existence of three typical kinds of ultrabroadband excitations whose profiles strongly depend upon their angular momenta. Looking forward to surveying their scattering features, we unearth some underlying head-on scenarios of elastic collisions. Accordingly, we address some useful and straightforward applications in nonlinear optics through secured data transmission systems, as well as laser physics and soliton theory with optical soliton dynamics.

DOI: 10.1103/PhysRevE.90.063203 PACS number(s): 42.65.Wi, 42.65.Re, 42.65.Tg, 42.81.Dp

I. INTRODUCTION

One trend in the development of modern laser physics and coherent nonlinear optics is the formation of light pulses with shorter and shorter durations. Advances made in the realm of laser technologies make it possible to perform experimental investigations into the processes of nonlinear interactions between matter and electromagnetic waves. Now pulses containing only few periods of electromagnetic oscillations can be generated in the laboratory [1].

The propagation of ultimately short pulses in a medium actually reveals its nonlinear properties owing to their high power $\sim 10^{13}$~W cm^{-2}. The short absolute duration of such pulses leads in turn to a delay in the medium's polarization response, i.e., to a dispersion effect. In the present work, we report some interesting properties of the silica optical fibers within the viewpoint of propagation of ultimately short excitations (USEs) in the medium.

As is well known in the literature, the tradeoff between the dispersion tendency to flatten the wave, and the nonlinearity tendency to increase the wave slope, can result in the formation of robust solitons, i.e., stable solitary waves that can propagate with a constant velocity and interact elastically with similar waves. These robust properties point to the possibility of effectively applying USEs to optical communication systems [2]. The possibility of soliton modes of propagation of such USEs in various nonlinear media stands to be one of the most important and interesting questions in this connection. Due to the fact that the well-developed nonlinear optics formalism of approximation of a slowly varying wave-field amplitude is inapplicable in extremely short durations, the theoretical analysis of physical phenomena arising in the interactions of USE becomes very complicated and delicate.

In nonlinear optics, the propagation equation governing the evolution of complex envelope of optical pulses plays a key role. Such an equation would contain only the first derivative with respect to the spatial coordinate along the propagation direction in the situation where the assumption of slowly varying envelopes is made. This offers in turn a great benefit with substantial smaller computational effort than Maxwell's wave equations [3]. Vector-polarized solitons represent a very important class of localized solutions as the nonlinear birefringence induced by the optical Kerr effect becomes significant and polarization evolution altered drastically [4]. This can provide a new dimension of laser parameters while allowing quantum control in molecules and nanostructures [5,6].

The conversion of envelope solitons described by the nonlinear Schrödinger equation and its modifications to wave solitons containing a few oscillation cycles is an interesting and important step in the theory of nonlinear wave phenomena [7]. In this context, Kartashov *et al.* [8] found a newly class of few-cycle solitary solutions of the wave equation with Kerr-type nonlinearity that describes the propagation of electromagnetic pulses of a circularly polarized field. In the present work, we aim at discussing the above analysis for the silica optical fiber dynamics within a well-defined frequency range of the visible. We want to show that the previous uniaxial fibers can support the propagation of an arbitrary typical polarization field described by USEs whose profiles strongly depend upon their angular momenta. We then need to study in detail the interacting features of these structures which, are very important in ultrafast communication systems with superdense information packing.

Accordingly, the paper is organized as follows. In Sec. II, focusing the study on the plane-wave dynamics propagating along the longitudinal axis of the aforementioned linear silica fiber, we derive the basic nonlinear system of equations describing the dynamics of each modal component of the electric field in an account of the short-wavelength perturbation. In this section, we pay particular interest to the fundamental field mode while transforming its governing dynamical equation to a simpler and more manageable one. In Sec. III, we present the results of our analysis and we make a discussion of these features while determining the shifts of the individual solitons

*vkuetche@yahoo.fr
†youssoufas@yahoo.fr
‡tckofane@yahoo.com

in interaction. The details of the derivation of these results are presented in the Appendix for a better understanding of the above features. Finally, in the last section, we end this work with a brief summary while addressing some underlying and straightforward applications in nonlinear optics through secured data transmission systems, as well as laser physics and soliton theory with optical soliton dynamics.

II. ELECTRIC FIELD MODAL SYSTEM

Considering a nonmagnetic dielectric isotropic medium, Maxwell's equations of the electromagnetic wave propagation in such a milieu are easily reduced to the form

$$\nabla \times \nabla \times \mathbf{E} + \mu_0 \mathbf{D}_{tt} = \mathbf{0}, \tag{1}$$

where vector $\mathbf{E}$ is the electric field of the light wave, electric induction $\mathbf{D}$ characterizes the response of the medium, and constant μ_0 is the magnetic permeability of vacuum. The variable t stands for the time coordinate. We also mention that the subscripts with respect to the spacetime variables refer to their partial derivatives.

Theoretical studies of extremely short waves are most fully developed for plane waves. This approximation is actually consistent with fundamental mode dynamics in guiding structures such as hollow-core waveguides when the input power is below the critical power for self-focusing, and also where it is possible to neglect the longitudinal field component. Based upon the above assumption where we consider vector $\mathbf{E}(x,t) = E^y(x,t)\mathbf{e}_y + E^z(x,t)\mathbf{e}_z$, unit vectors $\mathbf{e}_y$ and $\mathbf{e}_z$ spanning the perpendicular plane to the propagation axis, the wave equation (1) becomes

$$\mathbf{E}_{xx} - \mathbf{E}_{tt}/c^2 = \mu_0\big(\mathbf{P}^L_{tt} + \mathbf{P}^{NL}_{tt}\big), \tag{2}$$

where variable x denotes the spatial coordinate in the direction of propagation, and vector $\mathbf{P}^L$ represents the linear part of the medium polarization, expressed as (see Ref. [9] and references therein)

$$\mathbf{P}^L(x,t) = \varepsilon_0 \int_{-\infty}^{t} \chi^{(1)}(t-t')\mathbf{E}(x,t')\,dt', \tag{3}$$

in such a way that to enforce causality, the susceptibility $\chi^{(1)}$ must satisfy $\chi^{(1)}(t') = 0$ if $t' < 0$. Typically, for silica fibers and for light in the visible to mid-infrared range, the Fourier transform $\widehat{\chi}^{(1)}$ of the susceptibility $\chi^{(1)}$ can be expressed as [9]

$$\widehat{\chi}^{(1)}(\lambda) = \frac{0.696\lambda^2}{\lambda^2 - 0.0684^2} + \frac{0.4079\lambda^2}{\lambda^2 - 0.116^2} + \frac{0.8974\lambda^2}{\lambda^2 - 9.896^2}, \tag{4}$$

where λ is the wavelength of light satisfying to $0.25\ \mu\text{m} < \lambda < 3.5\ \mu\text{m}$. Within the infrared range 1600–3000 nm, Eq. (4) is approximated by [10]

$$\widehat{\chi}^{(1)}(\lambda) \simeq \widehat{\chi}^{(1)}_0 - \widehat{\chi}^{(1)}_2\lambda^2, \tag{5}$$

where $\widehat{\chi}^{(1)}_0 = 1.1104$ and $\widehat{\chi}^{(1)}_2 = 0.010\,63\ \mu\text{m}^{-2}$.

In general, in the case of few-cycle vector solitons with arbitrary polarization, the nonlinear part $\mathbf{P}^{NL}$ of the medium polarization appearing in Eq. (2) above satisfies [11,12]

$$\partial_t \mathbf{P}^{NL} = \alpha|\mathbf{E}|^2\mathbf{E}_t + \beta\mathbf{E} \times (\mathbf{E} \times \mathbf{E}_t), \tag{6}$$

with the constants α and β representing the cœfficients of the instantaneous nonlinearity of the medium polarization response. These parameters actually characterize the electronic and electronic-vibrational nonlinearity on the evolution of a light signal in a medium, respectively [13]. As the duration of ultrashort excitations decreases, the relative influence of the character of the self-action of the waves decreases significantly. In this context, the parameter β mentioned previously can be neglected. We note that for the case of a transparent medium as it is considered presently, the parameter α is always positive-valued, i.e., $\alpha > 0$ and proportional to the third-order susceptibility $\chi^{(3)}$ of the medium [14].

Based upon the approximation of the susceptibility given by Eq. (5), the Fourier transform of the linear part of Eq. (2) is given by

$$\widehat{\mathbf{E}}_{xx} + \big(1 + \widehat{\chi}^{(1)}_0\big)(\omega^2/c^2)\widehat{\mathbf{E}} - (2\pi)^2\widehat{\chi}^{(1)}_2\widehat{\mathbf{E}} = 0, \tag{7}$$

where the angular frequency $\omega = 2\pi c/\lambda$, and $\widehat{\mathbf{E}}$ is the Fourier transform of the field $\mathbf{E}$. Setting the constants $c_1 = c/\sqrt{1+\widehat{\chi}^{(1)}_0} \equiv 2.065 \times 10^8\ \text{ms}^{-1}$ and $c_2 = 1/2\pi\sqrt{\widehat{\chi}^{(1)}_2} \equiv 1.59\ \mu\text{m}$, we account for the nonlinear term in the polarization by taking the inverse Fourier transform of Eq. (7) so as to yield

$$\mathbf{E}_{xx} = \mathbf{E}_{tt}/c_1^2 + \mathbf{E}/c_2^2 + \alpha(|\mathbf{E}|^2\mathbf{E}_t)_t, \tag{8}$$

which stands for an accurate approximation of the reductive Maxwell's equation (1) of vector ultrabroadband optical waveguide channels propagating in the silica fiber within the 1600–300 nm wavelength regime.

For a better investigation of the wave propagation in the silica fiber above, it is suitable to get its linear behavior by sending in the medium a light wave of the form $\mathbf{A}\exp(\imath\omega t + \imath\kappa x)$ where constant vector $\mathbf{A}$ is arbitrary, and quantities ω and κ here stand for the angular frequency and the wave number of the plane wave. Also $\imath^2 = -1$. Hence, it becomes

$$\omega^2/c_1^2 = 1/c_2^2 + \kappa^2, \tag{9}$$

standing for the dispersion relation whose representation is depicted in Fig. 1. From this figure, when $\omega \to \infty$, the angular frequency is proportional to the wave number. We will be interested in studying this short-wave limit. Thus, suppose $\kappa \sim \kappa_0/\epsilon$ with $\epsilon \ll 1$, and furthermore that $\omega(\kappa)$ is bounded or has a pole of at least order one in κ; that is to say, we could write

$$\omega = \omega_{-1}/\epsilon + \omega_1\epsilon + \cdots. \tag{10}$$

This assumption corresponds just to the requirement that short waves exist in the linear limit. With such a dispersion relation, we have that the phase velocity and the group velocity are always bounded in the short-wave limit. This results to finite velocity propagation of geometrical characteristics and of energy. Thus, replacing the expression given by Eq. (10) into the dispersion relation above provides $\omega_{-1} = \pm c_1\kappa_0$ and $\omega_1 = \pm c_1/2c_2^2\kappa_0$. We note that the constant κ_0 can be calculated as $\kappa_0 = 2\pi/\lambda_0$ with $\lambda_0 = 9.896\ \mu\text{m}$. Consequently, the phase $\imath(\omega t + \kappa x) \equiv \imath\kappa_0(x \pm c_1 t)\epsilon^{-1} + \imath\omega_1(\epsilon t)$. With such an expression, we can introduce two independent variables X and T defined as

$$X = (x \pm c_1 t)/\epsilon, \quad T = t\epsilon, \tag{11}$$

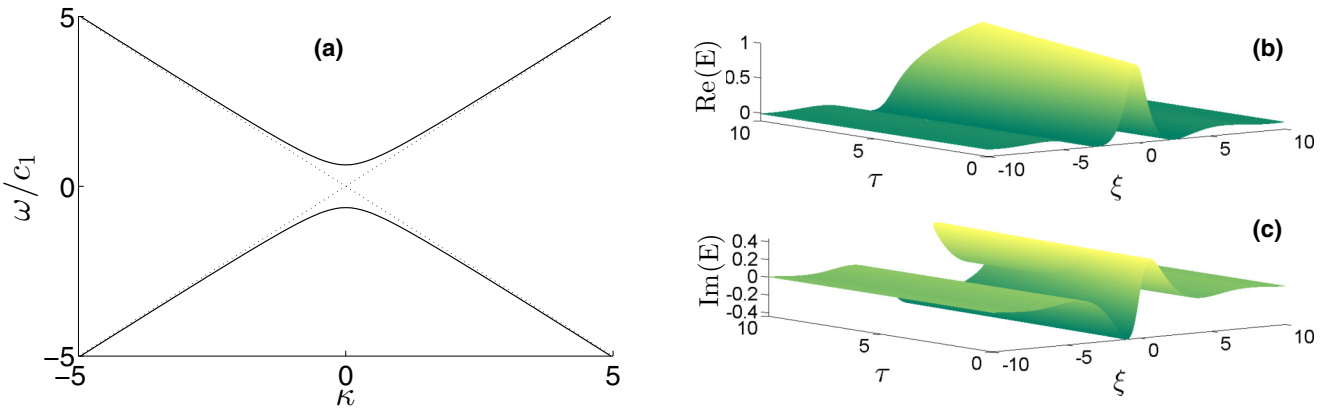

FIG. 1. (Color online) Dispersion relation and wave steepening. (a) Dispersion relation; (b, c) 3D representation of the steepening of an initially singlevalued profile to a multivalued one. In the numerics, we have arbitrarily considered the initial condition $E(\xi,0) = \exp(\imath\xi)/\left(1+\xi^2\right)$.

to study in detail the full nonlinear system. Accordingly, it is suitable to expand the vector field $\mathbf{E}$ as $\mathbf{E} = \sum_{n=1}^{\infty} \mathbf{E}_n \epsilon^n$ for ultrabroadband optical excitations. Thus, transforming Eq. (8) in terms of the new variables above while collecting the terms of order ϵ^n, $n = 1,2,3,\ldots$, we obtain the generic governing equation of each mode $\mathbf{E}_n$ as follows:

$$-(2/\sigma)\mathbf{E}_{n,\mathrm{XT}} = \mathbf{E}_n/c_2^2 + \mathbf{E}_{n-2,TT}/\sigma^2 + \alpha\left(\sum_{m=4}^{n-1}\sum_{l=3}^{m-1}(\mathbf{E}_{n-m}\cdot\mathbf{E}_{m-l}\mathbf{E}_{l-2,T})_T + 2\sigma\sum_{m=2}^{n-1}\sum_{l=1}^{m-1}(\mathbf{E}_{n-m}\cdot\mathbf{E}_{m-l}\mathbf{E}_{l,X})_T + \sigma^2\sum_{m=0}^{n-1}\sum_{l=-1}^{m-1}(\mathbf{E}_{n-m}\cdot\mathbf{E}_{m-l}\mathbf{E}_{l+2,X})_X\right), \tag{12}$$

where constant $\sigma = \pm c_1$. As a matter of illustration, we provide below the equations for the three first modes, i.e., $n = 1$, $n = 2$, and $n = 3$:

(i) For $n = 1$, we find

$$-(2/\sigma)\mathbf{E}_{1,\mathrm{XT}} = \mathbf{E}_1/c_2^2 + \alpha\sigma^2(|\mathbf{E}_1|^2\mathbf{E}_{1,X})_X. \tag{13}$$

This fundamental mode can also be derived from the viewpoint of another physical onset based upon the excitation-dependent refractive index of a two-level system (TLS) [15]. In this base point, the reduced Maxwell-Bloch equations are derived, accordingly. The mathematical equivalence is achieved under the assumption that the TLS polarization $P_{\mathrm{TLS}} = d_{21}\rho_{12} + d_{12}\rho_{21}$ is proportional to $|\mathbf{E}|^2\mathbf{E}_t$, where d_{12} and d_{21} are elements of the dipole matrix, and ρ_{ij} $(i,j = 1,2)$ is the density matrix of the TLS. However, this condition does not hold systematically for all material and details need to be specified structurally in order to ensure such an assumption.

(ii) For $n = 2$, we find

$$-(2/\sigma)\mathbf{E}_{2,\mathrm{XT}} = \mathbf{E}_2/c_2^2 + \alpha\sigma^2[(|\mathbf{E}_1|^2\mathbf{E}_{2,X})_X + 2(\mathbf{E}_1\cdot\mathbf{E}_2\mathbf{E}_{1,X})_X]. \tag{14}$$

(iii) For $n = 3$, we find

$$-(2/\sigma)\mathbf{E}_{3,\mathrm{XT}} = \mathbf{E}_3/c_2^2 + \mathbf{E}_{1,TT}/\sigma^2 + \alpha\sigma^2[(|\mathbf{E}_1|^2\mathbf{E}_{3,X})_X + (|\mathbf{E}_2|^2\mathbf{E}_{1,X})_X + (2/\sigma)(|\mathbf{E}_1|^2\mathbf{E}_{1,X})_T + 2(\mathbf{E}_1\cdot\mathbf{E}_3\mathbf{E}_{1,X})_X + 2(\mathbf{E}_1\cdot\mathbf{E}_2\mathbf{E}_{2,X})_X]. \tag{15}$$

The process can continue for $n \geqslant 4$.

We pay particular interests to the fundamental mode $n = 1$, which actually stands for the "seed" mode of the whole system. In fact, getting inside its whole dynamics suffices to generate the other modes. This constitutes our present concern. Selecting arbitrarily the constant $\sigma = -c_1$ within Eq. (12), we derive the following complex-valued evolution equation:

$$E_\tau - (1/2)EE^\star E_\xi - \int_{-\infty}^{+\infty} \mathrm{K}(\xi - s)E_s(s,\tau)\,ds = 0, \tag{16}$$

provided $E = E_1^y + \imath E_1^z$ $(\imath^2 = -1)$, $\xi = X/(c_1c_2\sqrt{2\alpha})$, and $\tau = (c_1^2\sqrt{\alpha/2})T/c_2$. Note that the star $(\star)$ symbol refers to the complex conjugation. The function K represents the kernel of the above integral term defined by $\mathrm{K}(s) = |s|/2$. The introduction of the kernel actually assumes that the observable E asymptotically decreases rapidly. The form given by Eq. (16) is very convenient for a proper discussion of the existence of traveling waveguide excitations which would result from the tradeoff between the nonlinearity and the dispersion.

Let us provide a straightforward analysis of the system (16). We consider a single model equation given by

$$E_\tau - (1/2)EE^\star E_\xi = 0, \tag{17}$$

which is free from any dispersion and dissipation. Thus, any initial smooth solution with vanishing boundary conditions, i.e., $\lim_{\xi\to\pm\infty} E = 0 + \imath 0$, becomes ambiguous in the final analysis. This stems from the dependency of the absolute wave-front velocity to the square amplitude $EE^\star$. A graphical representation of such features is depicted at Fig. 1 showing how an initial single-valued profile deforms or steepens as time

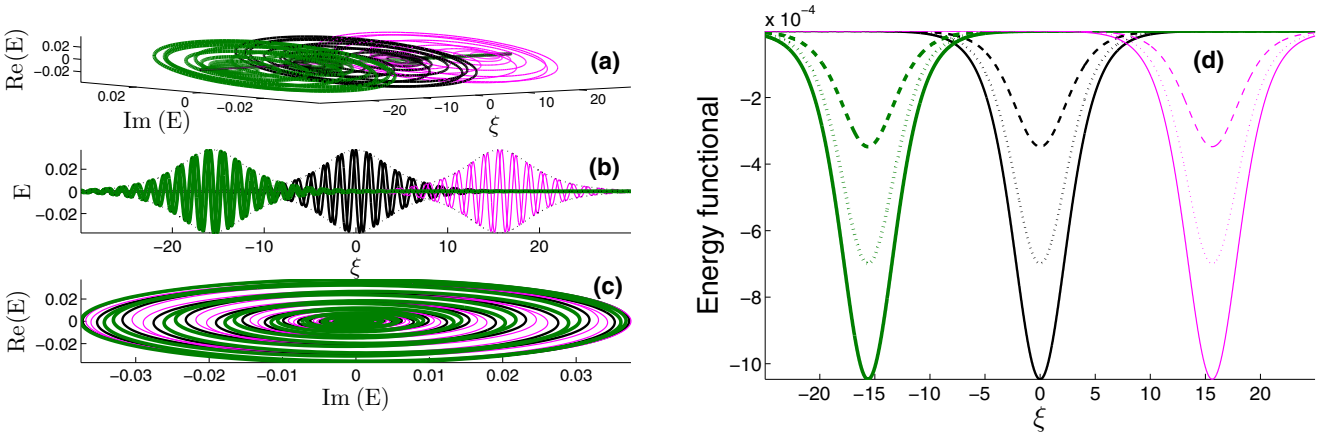

FIG. 2. (Color online) Rotating one-breather-like soliton with hump envelope depicted at times $\tau = -250, 0, 250$ (a, b, c) corresponding to three moving states represented by magenta (thin line), black (small thickness), and green (large thickness), respectively. The parameters $\mu = 4$ and $\mathrm{Re}(\kappa) = 0.3$ are selected such that the computed angular velocity of such a solitary wave is $\Omega = 0.2493$. The energy functional of these waves is depicted in panel (d) with the specified colors above. The solid line, dotted line, and broken line refer to their total energy, kinetic energy, and potential energy densities, respectively.

elapses and at the final analysis becomes multivalued. Now, when the dissipation $\rho E_{\xi\xi}$ (constant $\rho \neq 0$) is considered, the resulting equation becomes the modified complex-valued Burgers system [16]. The inclusion of this dissipative term transforms the solutions so that they cannot be ambiguous as a result of evolution. Following this analysis, the question logically arises whether the inclusion of the integral term would give rise to unambiguous solutions or rather coherent profiles. From the mathematical point of view, the ambiguous solutions do not present difficulties while the physical interpretation of ambiguity always has some difficulties. Thus, the problem of ambiguous solutions is regarded to be underlying. It is actually questionable whether the ambiguity has a physical nature or is related to the incompleteness of mathematical models, particularly to the lack of dissipation.

III. RESULTS AND DISCUSSIONS

In order to properly investigate the variations of the first modal electric field above, we use Hirota's bilinearization method [17] under the boundary conditions $E \to 0 + \imath 0$ as $\xi \to \pm\infty$. Accordingly, it seems straightforward to try the solutions to Eq. (16) of the form $E = G/F$ with $\xi = y - 2(\ln F)_\tau + \xi_0$ where constant ξ_0 is an arbitrary parameter, and the dependent functions G and F satisfy the bilinear equations $D_y D_\tau G \cdot F = GF$ and $D_\tau^2 F \cdot F = GG^\star/2$, symbols D_y and D_τ referring to Hirota's operators [16] with respect to the arbitrary implicit variable y and time τ, respectively. The motivation of choosing the form of E has been pointed out previously while discussing the effect of nonlinearity. According to the usual procedure, the dependent functions G and F should be expanded into suitable power series of a perturbation parameter. In addition, Eq. (16) has a canonical formulation: the Lagrangian $\mathcal{L}$ and the Hamiltonian $\mathcal{H}$ of the system can easily be found. Noticing that the system is natural, the potential $\mathcal{V}$ and the kinetic $\mathcal{T}$ energy densities of the system derive straightforwardly from the relations $\mathcal{V} = (\mathcal{H} - \mathcal{L})/2$ and $\mathcal{T} = (\mathcal{H} + \mathcal{L})/2$. Actually, the individual excitations parameters are explicitly given by the complex-valued wave number $\kappa = \mathrm{Re}(\kappa) + \imath\sqrt{\mu^2 - \mathrm{Re}(\kappa)^2}$ and frequency $\omega = v\mathrm{Re}(\kappa) + \imath\Omega$ with constant μ being an arbitrary parameter. The linear velocity and the angular velocity are expressed as $v = -1/\mu^2$ and $\Omega = \sqrt{\mu^2 - \mathrm{Re}(\kappa)^2}/\mu^2$, respectively. It should be noted that $-\mu \leqslant \mathrm{Re}(\kappa) \leqslant \mu$, provided $\mu > 0$. The discussion below of the different features depicted by the electric field E is done in account of the different values taken by the above parameters with respect to the "single" wave motion of the observable E and its scattering scenarios.

While determining the operator $\partial_\xi = \partial_y/[1 - 2(\ln F)_{\tau y}]$, it appears straightforward to introduce a parameter $\overline{\lambda}$ defined as $\overline{\lambda} = -2v\mathrm{Re}(\kappa)^2$. Accordingly, we found three important cases to be properly investigated:

(a) For $\overline{\lambda} < 1$, the rotating one-soliton solution has the form of a breather with hump envelope in such a way that the parameter $\mathrm{Re}(\kappa)$ satisfies to the following condition $-\mu/\sqrt{2} \leqslant \mathrm{Re}(\kappa) \leqslant \mu/\sqrt{2}$. The illustration is presented in Fig. 2 showing the breather states with hump envelope at $\tau = -250$, $\tau = 0$, and $\tau = 250$ associated to magenta (thin line), black (small thickness) and green (large thickness), respectively. The angular velocity of these waveguide channels is given by $\Omega = 0.2493$ showing that they rotate clockwise around the ξ axis. The energy functional of these waves is depicted in Fig. 2 showing a negative-valued potential energy which actually ascribes a relative stability to such a waveguide channel.

(b) For $\overline{\lambda} = 1$, the rotating one-soliton solution has the form of a breather with cusp envelope in such a way that the parameter $\mathrm{Re}(\kappa)$ satisfies $\mathrm{Re}(\kappa) = \pm\mu/\sqrt{2}$. The illustration is presented in Fig. 3 showing the breather states with cusp envelope at $\tau = -20$, $\tau = 0$, and $\tau = 20$ associated to magenta (thin line), black (small thickness) and green (large thickness), respectively. The angular velocity of these waveguide channels is given by $\Omega = 0.1768$ showing that they rotate clockwise around the ξ axis. The energy functional of these waves is depicted in Fig. 3 showing a negative-valued potential energy which actually ascribes a relative stability to such a waveguide channel. However, comparing the two

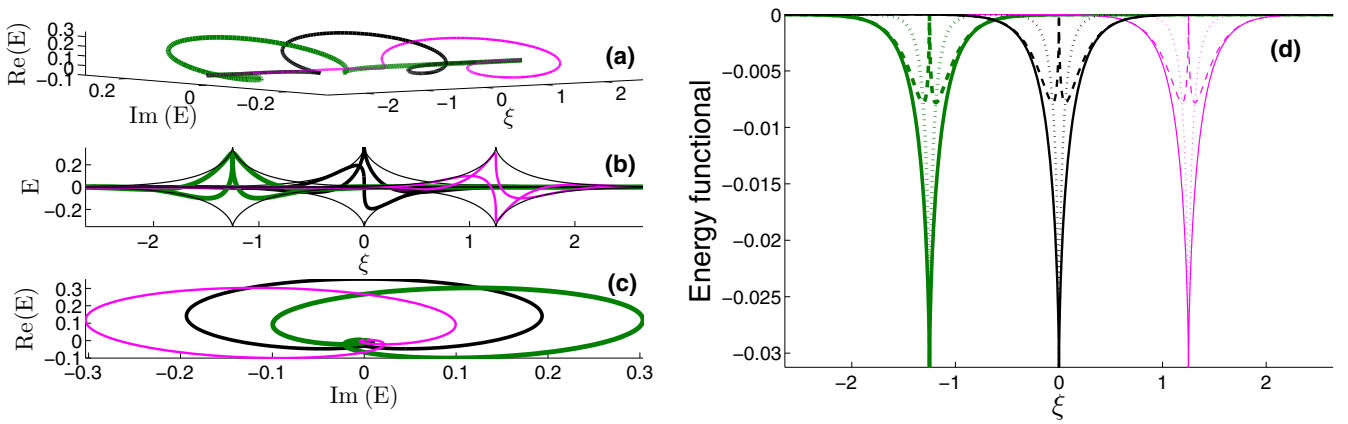

FIG. 3. (Color online) Rotating one-breather-like soliton with cusp envelope (thin black line) depicted at times $\tau = -20, 0, 20$ (a, b, c) corresponding to three moving states represented by magenta (thin line), black (small thickness), and green (large thickness), respectively. The parameters $\mu = 4$ and $\mathrm{Re}(\kappa) = 2.8284$ are selected such that the computed angular velocity of such a solitary wave is $\Omega = 0.1768$. The energy functional of these waves is depicted in panel (d) with the specified colors above. The solid line, dotted line, and broken line refer to their total energy, kinetic energy, and potential energy densities, respectively.

potential energies above, it appears that the first configuration is the most stable one.

(c) For $\bar{\lambda} > 1$, the rotating one-soliton solution has the form of a loop in such a way that the parameter $\mathrm{Re}(\kappa)$ satisfies the following condition $\mathrm{Re}(\kappa) \in]-\mu, -\mu/\sqrt{2}[\cup]\mu/\sqrt{2}, \mu[$. The illustration is presented in Fig. 4 showing the breather states at $\tau = -250$, $\tau = 0$, and $\tau = 250$ associated to magenta (thin line), black (small thickness) and green (large thickness), respectively. The angular velocity of these waveguide channels is given by $\Omega = 0.0556$ showing that they rotate clockwise around the ξ axis. The energy functional of these waves is depicted in Fig. 4 showing a potential energy likely to take negative or positive values with respect to the propagating amplitudes. Thus, comparing the potential energies above, it appears that this configuration is less stable than the first ones.

One physical comment which stems from the above profiles is that the electric field excitations can be produced as short as to reach a one-cycle period as shown in Fig. 3. However, though the energy functionals show that the most stable profile is that of Fig. 2, by tuning suitably the parameter $1/\mathrm{Re}(\kappa)$ to small values, i.e., reducing the length of the wave train significantly, one would hence generate a very shorter single-valued light wave for an ultrabroadband optical soliton very close to the one presented in Fig. 3. Now, concerning the multivalued wave of Fig. 4, it is actually questionable whether the silica optical fiber would support such an excitation. As far as we are concerned, no experimental investigation of such kind of structures in optics propagation has been reported. However, in a recent pioneering analysis, some complex multivalued excitations have been unearthed in the light fields analytically by Kedia *et al.* [18] as a new family of null solutions to Maxwell's equations in free space whose field lines encode all torus knots and links. Actually, the relation between the multivalued solutions above and the knot solutions derived by Kedia *et al.* [18] are not well founded owing to the fact that knot solutions are essentially three-dimensional. Nonetheless, the existence of the knot solutions indicates that even singular short waves with infinite derivatives at some localized points can be solutions to the Maxwell's equations. While the question logically arises whether the lower-dimensional Maxwell's

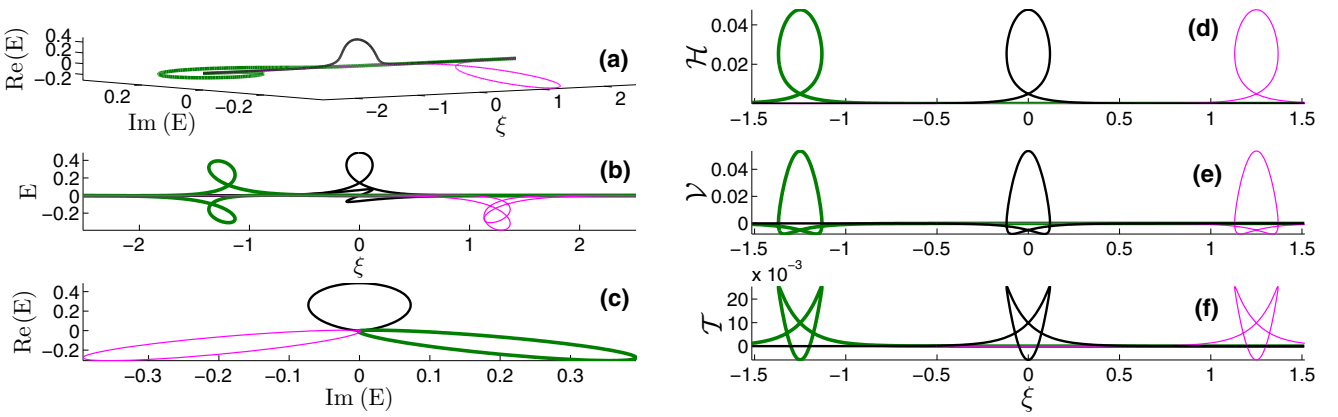

FIG. 4. (Color online) Rotating one-loop soliton solution depicted at times $\tau = -20, 0, 20$ (a, b, c) corresponding to three moving states represented by magenta (thin line), black (small thickness), and green (large thickness), respectively. The following parameters $\mu = 4$ and $\mathrm{Re}(\kappa) = 3.9$ are selected such that the computed angular velocity of such a solitary wave is $\Omega = 0.0556$. The energy functional of these waves is depicted in panels (d), (e), and (f) with the specified colors above.

equations can support such ambiguous short waves, Sazonov and Ustinov [19] investigated recently the propagation of extremely short looplike solitons in a "biaxial" crystal under the conditions of conical refraction. They performed the physical analysis of these multivalued waves while reporting their physical sense for the one-dimensional medium (optical fiber). However, the worth interesting and challenging work to do is to setup experiments in the context in order to measure experimentally the time durations of such short waves, and then compare with the analytical values. This is currently under investigation.

Now, let us analyze how the above traveling structures would behave in the silica optical fiber when they head-on to each other. This analysis would actually open some interesting perspectives in the area of optical communication systems. In such a context, we first discuss the space shifts of each interacting excitations. The problem is addressed in terms of an asymptotical consideration of the expression of the two-soliton solution to the previous system. Thus, we assume that $v_2 < v_1$ [with $\mathrm{Re}(\kappa_m) > 0, m = 1,2$] meaning that the soliton 2 is moving faster than the soliton 1. With such an hypothesis which does not breakdown the generality, the shifts δ_1 and δ_2 of the previous solitons expressed within the (ξ,τ) coordinates are easily found in the following way.

(i) We consider that only the phase $\mathrm{Re}(\theta_2)$ varies. Naturally, the phase $\mathrm{Re}(\theta_1)$ is constant.

(a) In the limit $\tau \to -\infty$, i.e., $\mathrm{Re}(\theta_2) \to +\infty$, it becomes

$$E \to \frac{C_2 \exp[\iota \mathrm{Im}(\theta_1) - \delta_{11} - \delta_{12}]}{2A_2} \mathrm{sech}\,[\mathrm{Re}(\theta_1)+\delta_{11}+\delta_{12}]\,, \tag{18a}$$

$$z \to y - 4\mathrm{Re}(\omega_2) - 2\partial_\tau \ln[1+\exp(2\mathrm{Re}(\theta_1)+2\delta_{11}+2\delta_{12})], \tag{18b}$$

where $\delta_{11} = (1/2)\ln A_1$ and $\delta_{12} = (1/2)\ln(B_{12}/A_1A_2)$.

(b) In the limit $\tau \to +\infty$, i.e., $\mathrm{Re}(\theta_2) \to -\infty$, it becomes

$$E \to \frac{\exp[\iota \mathrm{Im}(\theta_1) - \delta_{11}]}{2} \mathrm{sech}\,[\mathrm{Re}(\theta_1) + \delta_{11}]\,, \tag{19a}$$

$$z \to y - 2\partial_\tau \ln\{1 + \exp[2\mathrm{Re}(\theta_1) + 2\delta_{11}]\}\,. \tag{19b}$$

Consequently, the phase-shift of the soliton moving with velocity v_1 is

$$\mathrm{Re}(\Delta\phi_1) = -4\mathrm{Re}(\kappa_1)\mathrm{Re}(\omega_2) + \frac{1}{2}\ln\left(\frac{B_{12}}{A_1A_2}\right),$$
$$\mathrm{Im}(\Delta\phi_1) = -4\mathrm{Im}(\kappa_1)\mathrm{Re}(\omega_2) - \iota \ln\left[\frac{A_{12}(\omega_1-\omega_2)^2}{|A_{12}||\omega_1-\omega_2|^2}\right]. \tag{20}$$

The term $\mathrm{Re}(\Delta\phi_1)$ represents the shift due to nonlinear interactions in the $(y-\tau)$ spacetime, while the other term $\mathrm{Im}(\Delta\phi_1)$ is due to rotation. Returning to the initial variables ξ and τ, the shift in space of the previous soliton is hence

$$\delta_1 = -4\mathrm{Re}(\omega_2) + \frac{1}{2\mathrm{Re}(\kappa_1)}\ln\left(\frac{B_{12}}{A_1A_2}\right). \tag{21}$$

(ii) We now consider that only the phase $\mathrm{Re}(\theta_1)$ varies.

(a) In the limit $\tau \to -\infty$, i.e., $\mathrm{Re}(\theta_1) \to -\infty$, it becomes

$$E \to \frac{\exp[\iota \mathrm{Im}(\theta_2) - \delta_{22}]}{2} \mathrm{sech}\,[\mathrm{Re}(\theta_2) + \delta_{22}]\,, \tag{22a}$$

$$z \to y - 2\partial_\tau \ln\{1 + \exp[2\mathrm{Re}(\theta_2) + 2\delta_{22}]\}\,, \tag{22b}$$

where $\delta_{22} = (1/2)\ln A_2$.

(b) In the limit $\tau \to +\infty$, i.e., $\mathrm{Re}(\theta_1) \to +\infty$, it becomes

$$E \to \frac{C_1 \exp[\iota \mathrm{Im}(\theta_2) - \delta_{22} - \delta_{12}]}{2A_1} \mathrm{sech}\,[\mathrm{Re}(\theta_2)+\delta_{12}+\delta_{22}]\,, \tag{23a}$$

$$z \to y - 4\mathrm{Re}(\omega_1) - 2\partial_\tau \ln\{1+\exp[2\mathrm{Re}(\theta_2)+2\delta_{12}+2\delta_{22}]\}\,. \tag{23b}$$

Hence, the phase shift of the soliton moving with velocity v_2 is

$$\mathrm{Re}(\Delta\phi_2) = -4\mathrm{Re}(\kappa_2)\mathrm{Re}(\omega_1) + \frac{1}{2}\ln\left(\frac{B_{12}}{A_1A_2}\right),$$
$$\mathrm{Im}(\Delta\phi_2) = -4\mathrm{Im}(\kappa_2)\mathrm{Re}(\omega_1) + \iota \ln\left[\frac{A_{12}(\omega_1-\omega_2)^2}{|A_{12}||\omega_1-\omega_2|^2}\right]. \tag{24}$$

The term $\mathrm{Re}(\Delta\phi_2)$ represents the shift due to nonlinear interactions in the $(y-\tau)$ spacetime, while the other term $\mathrm{Im}(\Delta\phi_2)$ is due to rotation. Returning to the initial variables ξ and τ, the shift in space of the previous soliton is hence

$$\delta_2 = 4\mathrm{Re}(\omega_1) - \frac{1}{2\mathrm{Re}(\kappa_2)}\ln\left(\frac{B_{12}}{A_1A_2}\right). \tag{25}$$

In Eqs. (21) and (25), the first term of the shift is due to two rotating solitons repelling, attracting each other, or traveling along another. The second terms show the shift caused by the nonlinear interaction between the solitons. The ratio of the amplitude of these interacting waves is given by $r = \mathrm{Re}(\omega_2)/\mathrm{Re}(\omega_1)$. For the discussion of the interacting features, we arbitrarily select $\mu_1 = 4$ and $\mu_2 = 2$. This leads to the ratio $r = 4\mathrm{Re}(\kappa_2)/\mathrm{Re}(\kappa_1)$. The graphical representation of the previous shifts is presented at Fig. 5 showing that the slower soliton always shifts forwards while the faster soliton can shift forwards or backwards depending upon the ratio of their amplitudes.

As an illustration of the previous analysis, a two-soliton solution feature is presented in Fig. 6 which describes the interaction between two rotating breathers with humplike envelope $\mathrm{Re}(\kappa_1) = 0.3$ and $\mathrm{Re}(\kappa_2) = 0.2$ of dissimilar amplitudes with ratio $r = 2.6667$. As we can see in this figure, the two single solitary waves seem to attract each other while moving to the left-hand side of the ξ axis. In fact, the larger breather overtakes the small one, and they all overlap in the scattering area. During this process, they shift forwards with $\delta_1 = 0.0060$ and $\delta_2 = 0.2160$ as materialized by the density plot, and at the end of the analysis, they recover their initial shapes. The angular velocities of these waveguide channels are given by $\Omega_1 = 0.2493$ and $\Omega_2 = 0.4975$ showing that the larger soliton precesses greatly than the other as they propagate.

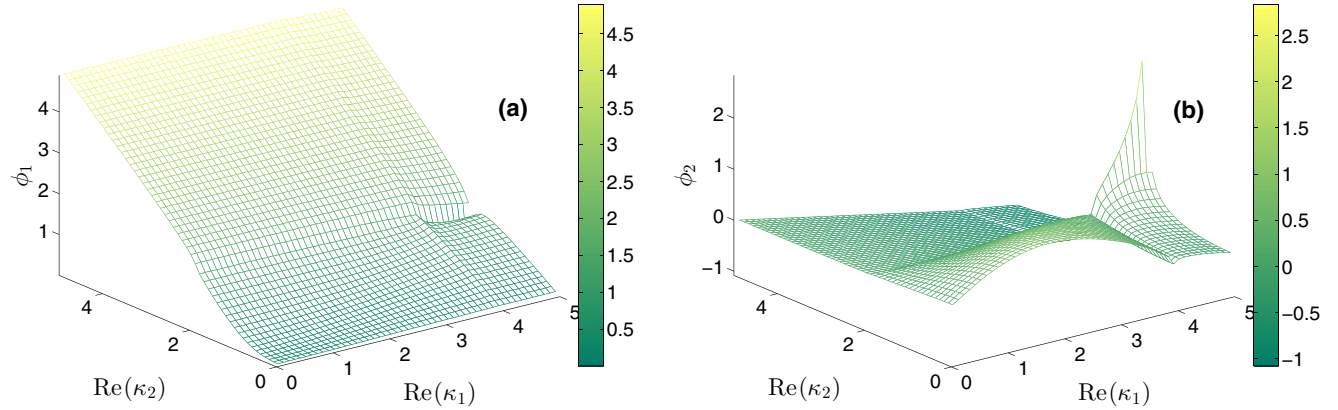

FIG. 5. (Color online) Shifts δ_1 and δ_2 of the interacting waveguide channels solutions. From this figure, the shift δ_1 (a) is always positive-valued meaning that the slower soliton is always shifted forwards by the interaction. The faster soliton can however shift forwards or backwards (b).

In the wake of the above features, another kind of two-soliton solution feature is presented in Fig. 7 which describes the interaction between two rotating breathers with cusplike envelope $\mathrm{Re}(\kappa_1) = 2.8284$ and $\mathrm{Re}(\kappa_2) = 1.414$ of dissimilar amplitudes with ratio $r = 2$. As we can see in this figure, the two single solitary waves attract each other while moving to the left-hand side of the ξ axis in such a way that the larger breather overtakes the small one and they all overlap in the scattering area. During this process, they shift forwards with $\delta_1 = 0.8452$ and $\delta_2 = 0.4309$ as materialized by the density plot, and at the end of the analysis, they recover their initial shapes. The angular velocities of these waveguide channels are given by $\Omega_1 = 0.1768$ and $\Omega_2 = 0.3536$ showing that the larger soliton precesses greatly than the other as they propagate.

Finally, we examine in Fig. 8 a typical kind of two-soliton solution feature which describes the interaction between two rotating multivalued solitons [20] $\mathrm{Re}(\kappa_1) = 3.9$ and $\mathrm{Re}(\kappa_2) = 1.9$ of dissimilar amplitudes with ratio $r = 1.9487$. As we can see in this figure, the two single solitary waves attract each other while moving to the left-hand side of the ξ axis in such a way that the smaller soliton travels along the larger one before being shifted. During this process, they shift forwards with $\delta_1 = 1.3579$ and $\delta_2 = 0.1377$ as materialized by the density plot and at the end of the analysis, they recover their initial shapes. The angular velocities of these waveguide channels are given by $\Omega_1 = 0.0556$ and $\Omega_2 = 0.1561$ showing that the larger loop soliton precesses greatly than the other as they propagate.

Now, let us extend the previous results to the investigation of the asymptotical behavior of the three-soliton optical signal, a solution to the aforementioned system. In this context, without any loss of generality, we assume that $v_3 < v_2 < v_1$ [with $\mathrm{Re}(\kappa_m) > 0, m = 1,2,3$], meaning that soliton 3 is moving faster than the others. With such an hypothesis, the shifts δ_1, δ_2, and δ_3 of the previous solitons expressed within the (ξ,τ) coordinates are easily derived as follows:

(a) We consider that only the phases $\mathrm{Re}(\theta_2)$ and $\mathrm{Re}(\theta_3)$ vary.

(i) In the limit $\tau \to -\infty$, i.e., $\mathrm{Re}(\theta_2) \to +\infty$ and $\mathrm{Re}(\theta_3) \to +\infty$, it becomes

$$E \to \frac{\exp[\imath\,\mathrm{Im}(\theta_1) + \imath\psi - \delta_{11}]}{2}\,\mathrm{sech}\,[\mathrm{Re}(\theta_1) + \varphi_{123} + \delta_{11}]\,, \tag{26a}$$

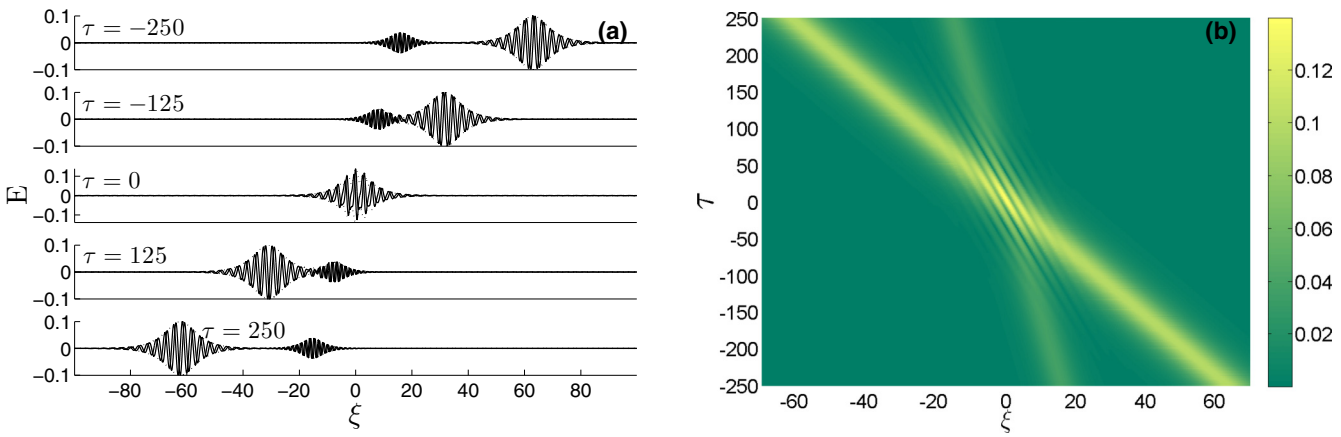

FIG. 6. (Color online) Rotating two-breather soliton with humplike envelope depicted within the time interval $-250 \leqslant \tau \leqslant 250$. These elastic interacting features are depicted with the selected parameters $[\mu_1 = 4, \mathrm{Re}(\kappa_1) = 0.3]$ and $[\mu_2 = 2, \mathrm{Re}(\kappa_2) = 0.2]$ such that the computed angular velocities of the interacting waves are $\Omega_1 = 0.2493$ and $\Omega_2 = 0.4975$. These amplitudes are dissimilar ($r = 2.6667$), and they shift forwards with a rate evaluated as $\delta_1 = 0.0060$ and $\delta_2 = 0.2160$ as depicted in the right-hand panel of the density plot.

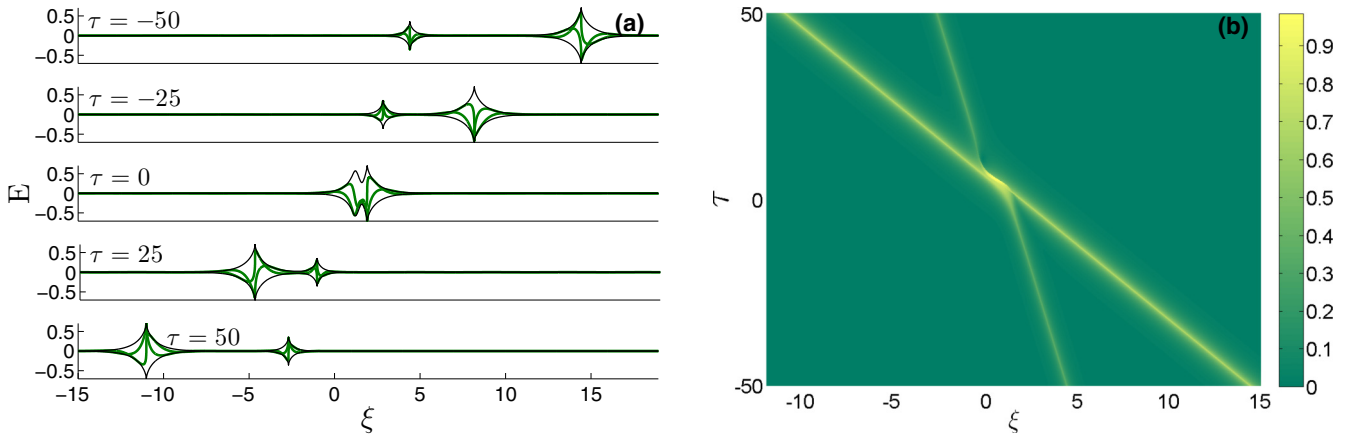

FIG. 7. (Color online) Rotating two-breather soliton with cusplike envelope (black color) depicted within the time interval $-50 \leqslant \tau \leqslant 50$. These elastic interacting features are depicted with the selected parameters $[\mu_1 = 4, \mathrm{Re}(\kappa_1) = 2.8284]$ and $[\mu_2 = 2, \mathrm{Re}(\kappa_2) = 1.414]$ such that the computed angular velocities of the interacting waves are $\Omega_1 = 0.1768$ and $\Omega_2 = 0.3536$. These amplitudes are dissimilar ($r = 2$), and they shift forwards with an amount rate evaluated as $\delta_1 = 0.8452$ and $\delta_2 = 0.4309$ as depicted in the right-hand panel of the density plot.

$$z \to y - 4\mathrm{Re}(\omega_2 + \omega_3) - 2\partial_\tau \ln\{1 + \exp[2\mathrm{Re}(\theta_1) + 2\varphi_{123} + 2\delta_{11}]\}, \tag{26b}$$

where $\delta_{11} = (1/2)\ln A_{11}$, $\psi = -\iota \ln(F_{12323}/|F_{12323}|)$ and $\varphi_{123} = \ln(|F_{12323}|/D_{2323})$.

(ii) In the limit $\tau \to +\infty$, i.e., $\mathrm{Re}(\theta_2) \to -\infty$, and $\mathrm{Re}(\theta_3) \to -\infty$, it becomes

$$E \to \frac{\exp[\iota \mathrm{Im}(\theta_1) - \delta_{11}]}{2} \mathrm{sech}\,[\mathrm{Re}(\theta_1) + \delta_{11}], \tag{27a}$$

$$z \to y - 2\partial_\tau \ln\{1 + \exp[2\mathrm{Re}(\theta_1) + 2\delta_{11}]\}. \tag{27b}$$

Consequently, the phase shift of the soliton moving with velocity v_1 is

$$\mathrm{Re}(\Delta\phi_1) = -4\mathrm{Re}(\kappa_1)\mathrm{Re}(\omega_2 + \omega_3) + \ln\left(\frac{|F_{12323}|}{D_{2323}}\right),$$
$$\mathrm{Im}(\Delta\phi_1) = -4\mathrm{Im}(\kappa_1)\mathrm{Re}(\omega_2 + \omega_3) - \iota \ln\left(\frac{F_{12323}}{|F_{12323}|}\right). \tag{28}$$

The term $\mathrm{Re}(\Delta\phi_1)$ represents the shift due to nonlinear interactions in the $(y - \tau)$ spacetime, while the other term $\mathrm{Im}(\Delta\phi_1)$ is due to rotation. Returning to the initial variables ξ and τ, the shift in space of the previous soliton is hence

$$\delta_1 = -4\mathrm{Re}(\omega_2 + \omega_3) + \frac{1}{\mathrm{Re}(\kappa_1)} \ln\left(\frac{|F_{12323}|}{D_{2323}}\right). \tag{29}$$

(b) We now consider that only the phases $\mathrm{Re}(\theta_1)$ and $\mathrm{Re}(\theta_3)$ vary.

(i) In the limit $\tau \to -\infty$, i.e., $\mathrm{Re}(\theta_1) \to -\infty$ and $\mathrm{Re}(\theta_3) \to +\infty$, it becomes

$$E \to \frac{\exp[\iota \mathrm{Im}(\theta_2) + \psi - \delta_{22}]}{2} \mathrm{sech}\,[\mathrm{Re}(\theta_2) + \varphi_{213} + \delta_{22}], \tag{30a}$$

$$z \to y - 4\mathrm{Re}(\omega_3) - 2\partial_\tau \ln\{1 + \exp[2\mathrm{Re}(\theta_2) + 2\varphi_{213} + 2\delta_{22}]\} \tag{30b}$$

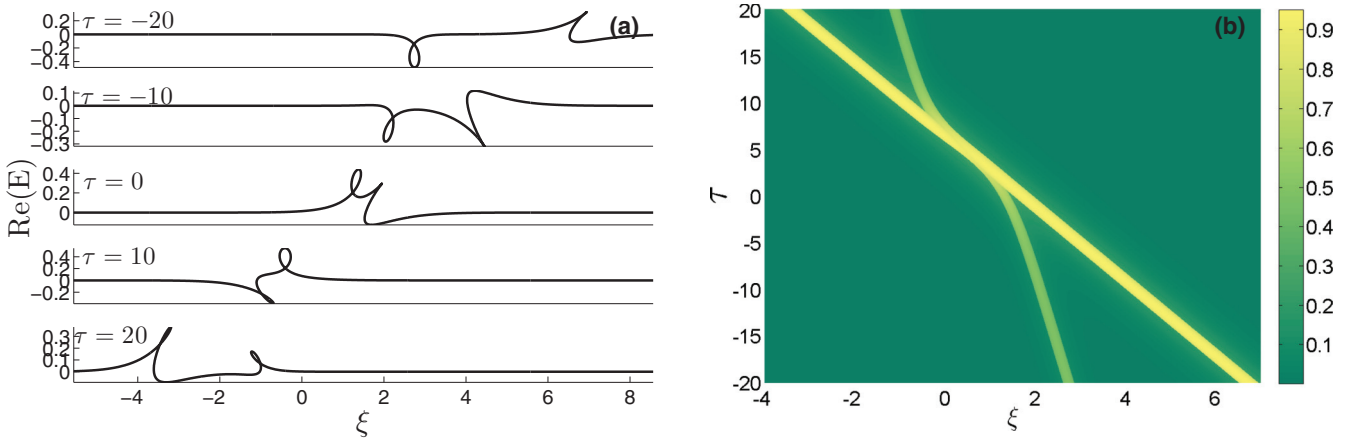

FIG. 8. (Color online) Rotating two-loop soliton depicted within the time interval $-20 \leqslant \tau \leqslant 20$. These elastic interacting features are depicted with the selected parameters $[\mu_1 = 4, \mathrm{Re}(\kappa_1) = 3.9]$ and $[\mu_2 = 2, \mathrm{Re}(\kappa_2) = 1.9]$ such that the computed angular velocities of the interacting waves are $\Omega_1 = 0.0556$ and $\Omega_2 = 0.1561$. These amplitudes are dissimilar ($r = 1.9487$), and they shift forwards with an amount rate evaluated as $\delta_1 = 1.3579$ and $\delta_2 = 0.1377$ as depicted in the right-hand panel of the density plot.

where $\delta_{22} = (1/2)\ln A_2$, $\psi = -\iota\ln(C_{233}/|C_{233}|)$, and $\varphi_{213} = \ln(|C_{233}|/A_{33})$.

(ii) In the limit $\tau \to +\infty$, i.e. $\mathrm{Re}(\theta_1) \to +\infty$ and $\mathrm{Re}(\theta_3) \to -\infty$, it becomes

$$E \to \frac{\exp[\iota\,\mathrm{Im}(\theta_2) + \psi' - \delta_{22}]}{2}\mathrm{sech}[\mathrm{Re}(\theta_2) + \varphi'_{213} + \delta_{22}], \tag{31a}$$

$$z \to y - 4\mathrm{Re}(\omega_1) - 2\partial_\tau \ln\{1 + \exp[2\mathrm{Re}(\theta_2) + \varphi'_{213} + 2\delta_{22}]\}, \tag{31b}$$

where $\psi' = -\iota\ln(C_{121}/|C_{121}|)$ and $\varphi'_{123} = \ln(|C_{121}|/A_{11})$. Hence, the phase shift of the soliton moving with velocity v_2 is

$$\mathrm{Re}(\Delta\phi_2) = 4\mathrm{Re}(\kappa_2)\mathrm{Re}(\omega_1 - \omega_3) - 2\ln\left(\frac{|C_{121}|A_{33}}{|C_{233}|A_{11}}\right),$$
$$\mathrm{Im}(\Delta\phi_2) = 4\mathrm{Im}(\kappa_2)\mathrm{Re}(\omega_1 - \omega_3) + \iota\ln\left(\frac{|C_{121}|C_{233}}{|C_{233}|C_{121}}\right). \tag{32}$$

The term $\mathrm{Re}(\Delta\phi_2)$ represents the shift due to nonlinear interactions in the $(y-\tau)$ spacetime, while the other term $\mathrm{Im}(\Delta\phi_2)$ is due to rotation. Returning to the initial variables ξ and τ, the shift in space of the previous soliton is hence

$$\delta_2 = 4\mathrm{Re}(\omega_1 - \omega_3) - \frac{1}{\mathrm{Re}(\kappa_2)}\ln\left(\frac{|C_{121}|A_{33}}{|C_{233}|A_{11}}\right). \tag{33}$$

(c) Finally, we consider that only the phases $\mathrm{Re}(\theta_1)$ and $\mathrm{Re}(\theta_2)$ vary.

(i) In the limit $\tau \to -\infty$, i.e., $\mathrm{Re}(\theta_1) \to -\infty$ and $\mathrm{Re}(\theta_3) \to -\infty$, it becomes

$$E \to \frac{\exp[\iota\,\mathrm{Im}(\theta_3) - \delta_{33}]}{2}\mathrm{sech}\,[\mathrm{Re}(\theta_3) + \delta_{33}]\,, \tag{34a}$$
$$z \to y - 2\partial_\tau \ln\{1 + \exp[2\mathrm{Re}(\theta_3) + 2\delta_{33}]\}\,, \tag{34b}$$

where $\delta_{33} = (1/2)\ln A_{11}$.

(ii) In the limit $\tau \to +\infty$, i.e., $\mathrm{Re}(\theta_1) \to +\infty$ and $\mathrm{Re}(\theta_2) \to +\infty$, it becomes

$$E \to \frac{\exp[\iota\,\mathrm{Im}(\theta_3) + \iota\chi - \delta_{33}]}{2}\mathrm{sech}\,[\mathrm{Re}(\theta_3) + \varphi_{312} + \delta_{33}]\,, \tag{35a}$$

$$z \to y - 4\mathrm{Re}(\omega_1 + \omega_2) - 2\partial_\tau \ln\{1 + \exp[2\mathrm{Re}(\theta_3) + 2\varphi_{312} + 2\delta_{33}]\}, \tag{35b}$$

where $\chi = -\iota\ln(F_{12312}/|F_{12312}|)$ and $\varphi_{312} = \ln(|F_{12312}|/D_{1212})$.

Consequently, the phase shift of the soliton moving with velocity v_3 is

$$\mathrm{Re}(\Delta\phi_3) = 4\mathrm{Re}(\kappa_3)\mathrm{Re}(\omega_1 + \omega_2) - \ln\left(\frac{|F_{12312}|}{D_{1212}}\right),$$
$$\mathrm{Im}(\Delta\phi_3) = 4\mathrm{Im}(\kappa_3)\mathrm{Re}(\omega_1 + \omega_2) + \iota\ln\left(\frac{F_{12312}}{|F_{12312}|}\right). \tag{36}$$

The term $\mathrm{Re}(\Delta\phi_3)$ represents the shift due to nonlinear interactions in the $(y-\tau)$ spacetime, while the other term $\mathrm{Im}(\Delta\phi_3)$ is due to rotation. Returning to the initial variables ξ and τ, the shift in space of the previous soliton is hence

$$\delta_3 = 4\mathrm{Re}(\omega_1 + \omega_2) - \frac{1}{\mathrm{Re}(\kappa_3)}\ln\left(\frac{|F_{12312}|}{D_{1212}}\right). \tag{37}$$

In Eqs. (29), (33), and (37), the first term of the shift is due to three rotating solitons repelling, attracting each other, or traveling along another. The second terms show the shift caused by the nonlinear interaction between the solitons.

For the discussion of the interacting features, we arbitrarily select $\mu_1 = 4$, $\mu_2 = 2$, and $\mu_3 = 1$. As illustration of the previous analysis, a three-soliton signal feature is presented in Fig. 9 which describes the interaction between three rotating breathers with humplike envelope [Fig. 9(a)] $\mathrm{Re}(\kappa_1) = 0.3$, $\mathrm{Re}(\kappa_2) = 0.2$, and $\mathrm{Re}(\kappa_2) = 0.1$ of dissimilar amplitudes. As depicted, the three single excitations attract each other while moving to the left-hand side of the ξ axis. In fact, the larger breather overtakes the small one and they all overlap in the scattering area. During this process, they shift forwards with $\delta_1 = 0.3619$, $\delta_2 = 0.2312$, and $\delta_3 = 0.6270$, and at the end of the analysis, they recover their initial shapes. The angular velocities of these waveguide channels are given by $\Omega_1 = 0.2493$, $\Omega_2 = 0.4975$, and $\Omega_3 = 0.9950$ showing that the larger soliton precesses greatly than the other as they propagate.

In the wake of the above features, one can render these wave trains as shorter as possible such as to generate ultrashort optical signals very important in nonlinear optics. Thus, a typical three-soliton feature is presented in Fig. 9 which describes the interaction between three rotating breathers with cusplike envelope [Fig. 9(b)] $\mathrm{Re}(\kappa_1) = 2.8284$, $\mathrm{Re}(\kappa_2) = 1.414$, and $\mathrm{Re}(\kappa_3) = 0.7071$ of dissimilar amplitudes. As depicted, the three single solitary waves attract each other while moving to the left-hand side of the ξ axis in such a way that the larger breather overtakes the small one and they all overlap in the scattering area. During this process, they shift forwards with $\delta_1 = 3.4488$, $\delta_2 = 2.1213$, and $\delta_3 = 1.0542$ such as recovering their initial shapes at the end of the analysis. The angular velocities of these waveguide channels are given by $\Omega_1 = 0.1768$, $\Omega_2 = 0.3536$, and $\Omega_3 = 0.7071$ showing that the larger soliton precesses greatly than the other as they propagate.

From a practical viewpoint, these elastic interaction between three optical excitations show that no matter complicated is the process in the scattering area, the silica fiber under the conditions specified previously actually supports the propagation of subsequent optical data under different rates of transmission with recovery of the initial properties. This useful property of the silica fiber opens perspectives in communication systems with data transmission elements in optical fiber. The additional parameter of angular momentum of the signals endows the process with a secure transmission.

IV. SUMMARY

In this paper, we have investigated the dynamics of an uniaxial silica fiber within the viewpoint of propagation of ultimately ultrashort optical waveguide channels. From the standpoint of a nonmagnetic dielectric isotropic medium, we have written Maxwell's equations of the electromagnetic wave propagation

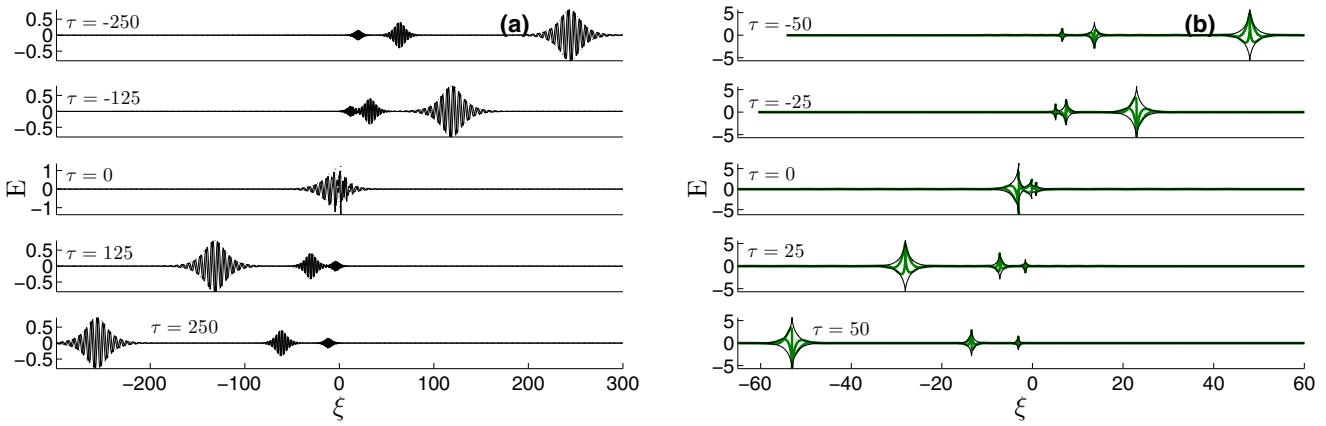

FIG. 9. (Color online) Rotating two-breather solitons: Humplike envelope (a) depicted within the time interval $-250 \leqslant \tau \leqslant 250$ and cusplike envelope (b) depicted within the time interval $-50 \leqslant \tau \leqslant 50$. These elastic interacting features are depicted with the following selected parameters: For panel (a), $[\mu_1 = 4, \mathrm{Re}(\kappa_1) = 0.3]$, $[\mu_2 = 2, \mathrm{Re}(\kappa_2) = 0.2]$, and $[\mu_2 = 1, \mathrm{Re}(\kappa_3) = 0.1]$ such that the computed angular velocities of the interacting waves are $\Omega_1 = 0.2493$, $\Omega_2 = 0.4975$, and $\Omega_3 = 0.9950$. For panel (b), $[\mu_1 = 4, \mathrm{Re}(\kappa_1) = 2.8284]$, $[\mu_2 = 2, \mathrm{Re}(\kappa_2) = 1.414]$, and $[\mu_2 = 1, \mathrm{Re}(\kappa_3) = 0.7071]$ such that the computed angular velocities of the interacting waves are $\Omega_1 = 0.1768$, $\Omega_2 = 0.3536$, and $\Omega_3 = 0.7071$. These amplitudes are dissimilar, and they shift forwards with an amount rate evaluated as $\delta_1 = 0.3619$, $\delta_2 = 0.2312$, and $\delta_3 = 0.6270$ for humplike envelopes, and $\delta_1 = 3.4488$, $\delta_2 = 2.1213$, and $\delta_3 = 1.0542$ for cusplike envelopes.

in such a milieu. Paying particular interest to a domain wavelength of light in the visible, i.e., $0.25\ \mu\mathrm{m} < \lambda < 3.5\ \mu\mathrm{m}$, we have reduced the initial equations to a lower-dimensional system expressed in terms of the electric field of the light wave. Using the reductive perturbation method of analysis, we isolated different modal states of the electric field, according to the perturbation orders involved. We paid attention to the fundamental mode of the electric field. We found that this field actually describes three kinds of ultrabroadband excitations whose profiles strongly depend upon their angular momenta. We studied the interactions between these structures, and we unearthed some underlying head-on scenarios showing elastic collision features. Discussing these features in depth, we computed the shifts of the individual solitons, and we found that they comprise two main terms: the first term characterizing the nonlinear interaction, and the second term due to two rotating solitons repelling, attracting each other or traveling along another. The energy functional analysis revealed that the wave train with a humplike envelope is the most stable. Nonetheless, by tuning suitably the parameter $1/\mathrm{Re}(\kappa)$ to small values, i.e., reducing the length of the wave train significantly, we would hence generate a very shorter single-valued light wave for an ultrabroadband optical soliton, very close to the cusplike envelope presented in Fig. 3. This generating process is actually very important both from the physical and practical issues in view of the considerable advances in laser technology in the generation of ultrashort light pulses as short as a few optical oscillation periods. Such USEs would hence have a number of wide potentialities for their scientific and engineering applications, among which possible superdense information packing with the use of such ultrashort waves and the corresponding ultrafast communications [1,21].

We would like to emphasize that our work is mainly and essentially physical though we made use of a powerful method, Hirota's bilinearization [18], to investigate the structural dynamics of the derived system (fundamental mode). This actually explains why we report all details of the calculus in the Appendix in view of focusing our interest mainly on the physical aspects. From a physical viewpoint, what is not known hitherto is the physical onsets of the propagation of ultrashort pulses with nonzero angular frequency within the silica fibers. For the first time, we derived a generic governing modal system ($n = 1,2,3,\ldots$) describing in detail the propagation of the previous rotating excitations. Though the physical onset of the Maxwell-Bloch equations for TLS can also lead to the two-component SW equation (fundamental mode), it is important to mention that only these features can be observed for a specific range of the incident electromagnetic waves. It is also worth mentioning that the governing coupled system (fundamental mode) that we derived casually has previously been reported by the present authors [22], though less investigated in detail at the time. At that current time, there was no any physical explanation of the derived system hitherto. Though this system has been subjected to further interests in different contexts (see Ref. [23] and references therein), we personally want to detail and engineer the calculus in the Appendix within the viewpoint developed in Ref. [22]. This is in view of computing explicitly the angular frequency of the propagating ultimately short waves along the fiber and to show that these waves depict different shapes with respect to the different values of their angular frequencies, but also for numerical computations of the subsequent modes. One important advantage of these results is the physical onset of the secured data transmission systems through rotation phenomenon and the angular momentum-dependent profiles of the interacting signals. In fact, in order to localize the propagating excitations, it is not sufficient to get only the position and the velocity of the waves. Thus, one needs to know about their nontrivial angular velocities.

In addition, another important result is that from one point to another in the transmission line, it is possible to send more than two signals moving with different velocities and

undergoing complicated interacting features, and then retrieve all these properties at the end point of the transmission optical line. Indeed, looking forward to getting more ideas about the interaction of more than two optical signals (fundamental modes) within the silica fiber, we found that in the range of light specified previously, that is, the domain wavelength of light in the visible, i.e., $0.25\ \mu\text{m} < \lambda < 3.5\ \mu\text{m}$, the signals interact elastically and preserve their initial properties while rotating along the optical fiber. The details for the interacting features of three optical signals along the silica fiber have been presented. The phase shifts of the individual signals are also determined in order to quantify the effects due to rotation and the nonlinearity. Though our work stands to be essentially physical, it actually offers further perspectives in the transmission data analysis within the framework of interactions of multisignals along the optical chain.

The results obtained for the fundamental mode ($n = 1$) and presented previously are actually and importantly useful for numerical computations of the subsequent modes $n = 2,3,4,\ldots$, in view of getting more ideas about the whole dynamics of the electric field in the silica optical fibers within the light range specified in the paper. This is currently under in-depth investigation within the computational approach developed by Skobelev and Kim [3,8], and the results will be reported in a separate paper. In addition, recently Yamane *et al.* [24] have proposed a high-precision method for measuring the orbital angular momentum spectrum of ultrabroadband optical-vortex pulses from forklike interferograms between OV pulses and a reference plane-wave pulse. It would hence be interesting to compare our computations to the experimental results to be obtained within the framework of the previous experimental method. This subject is currently under investigation and will be reported elsewhere.

The previous findings are actually of potential interest for applications to many areas of research, such as in nonlinear optics with the propagation of short-light excitations in nonlinear optical fibers, alongside quantum electronics, optoelectronics, and laser physics of extremely nonlinear optics [25], among others (see Refs. [3,26] and references therein). In soliton theory [17,27] where the characterization of the nonlinear scattering between the interacting waves (soliton network) is particularly underlying, understanding whether the interaction is elastic or not is very important within the viewpoint of the propagation of stable waveguide excitations in the system. This includes solitons in optical fibers for optical communication systems [14,28].

ACKNOWLEDGMENTS

The authors would like to express their sincere thanks to the anonymous referees for their critical comments and appropriate suggestions which have made this paper more precise and readable. V.K.K. is very grateful for the hospitality and the financial support for publication from the Abdus Salam International Centre for Theoretical Physics (ICTP, Trieste, Italy) where the present work has been initiated.

APPENDIX A: BILINEARIZATION

Let us introduce two independent variables $(y,\bar{t})$ such that $E(y,\bar{t})$ describes a single-valued function of y. It is convenient to set

$$\varphi dy = d\xi + EE^{\star}\, d\tau/2, \quad \bar{t} = \tau, \tag{A1}$$

where φ is an arbitrary function of $(y,\bar{t})$. Thus, Eq. (16) transforms to

$$E_{\bar{t}} = \int_{-\infty}^{+\infty} \mathrm{K}(\xi - s)E_s\, ds, \quad \varphi_{\bar{t}} = -(EE^{\star})_y/2. \tag{A2}$$

Setting $\varphi = z_y$, Eq. (A2) reads

$$E_{\bar{t}} = \int_{-\infty}^{+\infty} \mathrm{K}(\xi - s)E_s\, ds, \quad z_{\bar{t}y} = -(EE^{\star})_y/2, \tag{A3}$$

with $\xi = z + \xi_0$, ξ_0 being an arbitrary constant.

Equation (A3) has a canonical formulation. Indeed, noticing from Eq. (A3) that the expression $E_{y\bar{t}} = z_y \int_{-\infty}^{+\infty} K(\xi - s)E_{ss}\, ds$ holds, the Lagrangian $\mathcal{L}$ and the Hamiltonian $\mathcal{H}$ of the system are expressed as

$$\begin{aligned} \mathcal{L} &= \frac{E_{\bar{t}}E_y^{\star} + E_{\bar{t}}^{\star}E_y + 2z_y\,(z_{\bar{t}} + EE^{\star})}{4}, \\ \mathcal{H} &= 4[\gamma^y\gamma^{\bar{t}\star} + \gamma^{y\star}\gamma^{\bar{t}} + \chi^{\bar{t}}(\chi^y - EE^{\star}/2)/2], \end{aligned} \tag{A4}$$

where the generalized momenta γ^y, $\gamma^{\bar{t}}$, χ^y, and $\chi^{\bar{t}}$ read

$$\begin{aligned} &\gamma^y = E_{\bar{t}}^{\star}/4, \quad \gamma^{\bar{t}} = E_y^{\star}/4, \quad \chi^y = (z_{\bar{t}} + EE^{\star})/2, \\ &\chi^{\bar{t}} = z_y/2. \end{aligned} \tag{A5}$$

Equation (A3) is obtained from the Lagrangian system

$$\frac{\delta\mathcal{L}}{\delta E} = 0, \quad \frac{\delta\mathcal{L}}{\delta z} = 0. \tag{A6}$$

Since the system is natural, the potential $\mathcal{V}$ and the kinetic $\mathcal{T}$ energy densities read

$$\mathcal{V} = (\mathcal{H} - \mathcal{L})/2, \quad \mathcal{T} = (\mathcal{H} + \mathcal{L})/2. \tag{A7}$$

Equation (A3) can written into its bilinear form by means of the Hirota's method [17]. As a result, we derive

$$D_y D_{\bar{t}} G \cdot F = GF, \quad D_{\bar{t}}^2 F \cdot F = GG^{\star}/2, \tag{A8}$$

provided

$$E = G/F, \quad z = y - 2\,(\ln F)_{\bar{t}}\,. \tag{A9}$$

The symbols D_y and $D_{\bar{t}}$ refer to the Hirota's operators [17] with respect to the variable y and $\bar{t}$, respectively. According to the usual procedure, the dependent functions G and F are expanded into suitable power series of a perturbation parameter ϵ. In this paper, we arguably expand the functions G and F as follows:

$$\begin{aligned} G &= \epsilon G_1 + \epsilon^3 G_3 + \epsilon^5 G_5 + \cdots, \\ F &= 1 + \epsilon^2 F_2 + \epsilon^4 F_4 + \epsilon^6 F_6 + \cdots, \end{aligned} \tag{A10}$$

where the functions G_i, F_i, $(i = 1,2,3,\ldots)$ are expansion coefficients of the above series. Substituting this expansion into Eq. (A8) and collecting the terms of each order of ϵ, we obtain the results presented below.

APPENDIX B: SOLITON SOLUTIONS

1. The one-soliton solution

The one-soliton solution to Eq. (A8) is obtained from the following truncation:

$$G = \exp(\theta), \quad F = 1 + \exp(\theta + \theta^\star + 2\delta_0), \tag{B1}$$

where constant $\delta_0 = -\ln[4\mathrm{Re}(\omega)]$ with $2\mathrm{Re}(\omega) = \omega + \omega^\star$ and the phase θ is defined by

$$\theta = \omega\bar{t} - \kappa y + \theta_0, \tag{B2}$$

with constants κ and ω being complex-valued wave number and frequency of the traveling wave, and constant θ_0 being an arbitrary parameter. The dispersion relation reads $\omega\kappa = -1$. Solving the dispersion equation above, we find

$$\kappa = \mathrm{Re}(\kappa) + \imath\sqrt{\mu^2 - \mathrm{Re}(\kappa)^2}, \quad \omega = v\mathrm{Re}(\kappa) + \imath\Omega, \tag{B3}$$

where $\imath^2 = -1$, constant μ is an arbitrary parameter, and the linear velocity and the angular velocity are expressed as

$$v = -1/\mu^2, \quad \Omega = \sqrt{\mu^2 - \mathrm{Re}(\kappa)^2}/\mu^2. \tag{B4}$$

Thus, the traveling waves are left-moving. It should be noted that $-\mu \leqslant \mathrm{Re}(\kappa) \leqslant \mu$, provided $\mu > 0$.

From Eq. (A9), while determining the operator $\partial_\xi = \partial_y/[1 - 2(\ln F)_{y\bar{t}}]$, it is straightforward to introduce an arbitrary parameter $\overline{\lambda}$ defined as

$$\overline{\lambda} = -2v\mathrm{Re}(\kappa)^2, \tag{B5}$$

so as to discuss its different values.

2. The two-soliton solution

The two-soliton solution to Eq. (A8) is obtained from the following truncation:

$$F = 1 + A_1\exp[2\mathrm{Re}(\theta_1)] + A_2\exp[2\mathrm{Re}(\theta_2)] + A_{12}\exp(\theta_1 + \theta_2^\star) + A_{12}^\star\exp(\theta_1^\star + \theta_2) + B_{12}\exp[2\mathrm{Re}(\theta_1) + 2\mathrm{Re}(\theta_2)], \tag{B6a}$$

$$G = \exp(\theta_1) + \exp(\theta_2) + C_1\exp[\theta_2 + 2\mathrm{Re}(\theta_1)] + C_2\exp[\theta_1 + 2\mathrm{Re}(\theta_2)], \tag{B6b}$$

where

$$A_m = 1/16\mathrm{Re}(\omega_m)^2, \quad C_1 = 4(\omega_2 - \omega_1)^2 A_1 A_{12}^\star, \quad C_2 = 4(\omega_2 - \omega_1)^2 A_2 A_{12}, \tag{B7a}$$

$$A_{12} = 1/4(\omega_1 + \omega_2^\star)^2, \quad B_{12} = 16|\omega_2 - \omega_1|^4 A_1 A_2 |A_{12}|^2, \tag{B7b}$$

and $\omega_m = \omega_m\bar{t} - \kappa_m y + \theta_{0m}$ $(m = 1,2)$, θ_{0m} standing for arbitrary constants. The dispersion equation is given by $\omega_m\kappa_m + 1 = 0$ $(m = 1,2)$, from which a solution

$$\kappa_m = \mathrm{Re}(\kappa_m) + \imath\sqrt{\mu_m^2 - \mathrm{Re}(\kappa_m)^2}, \quad \omega_m = v_m\mathrm{Re}(\kappa_m) + \imath\Omega_m \tag{B8}$$

is derived and

$$v_m = -1/\mu_m^2, \quad \Omega_m = \sqrt{\mu_m^2 - \mathrm{Re}(\kappa_m)^2}/\mu_m^2, \quad (m = 1,2), \tag{B9}$$

which stands for the linear velocity and the angular velocity of the solitary wave of number m. It should be noted that $-\mu_m \leqslant \mathrm{Re}(\kappa_m) \leqslant \mu_m$, provided $\mu_m > 0$ $(m = 1,2)$.

3. The three-soliton solution

The three-soliton solution to Eq. (A8) is obtained from the following truncation:

$$\begin{aligned} G = {} & \exp(\theta_1) + \exp(\theta_2) + \exp(\theta_3) + C_{121}\exp[2\mathrm{Re}(\theta_1) + \theta_2] + C_{131}\exp[2\mathrm{Re}(\theta_1) + \theta_3] + C_{122}\exp[2\mathrm{Re}(\theta_2) + \theta_1] \\ & + C_{232}\exp[2\mathrm{Re}(\theta_2) + \theta_3] + C_{133}\exp[2\mathrm{Re}(\theta_3) + \theta_1] + C_{233}\exp[2\mathrm{Re}(\theta_3) + \theta_2] + C_{231}\exp(\theta_2 + \theta_3 + \theta_1^\star) \\ & + C_{132}\exp(\theta_1 + \theta_3 + \theta_2^\star) + C_{123}\exp(\theta_1 + \theta_2 + \theta_3^\star) + F_{12312}\exp[2\mathrm{Re}(\theta_1) + 2\mathrm{Re}(\theta_2) + \theta_3] \\ & + F_{12313}\exp[2\mathrm{Re}(\theta_1) + 2\mathrm{Re}(\theta_3) + \theta_2] + F_{12323}\exp[2\mathrm{Re}(\theta_1) + 2\mathrm{Re}(\theta_3) + \theta_1], \end{aligned} \tag{B10a}$$

$$\begin{aligned} F = {} & 1 + A_{11}\exp[2\mathrm{Re}(\theta_1)] + A_{22}\exp[2\mathrm{Re}(\theta_2)] + A_{33}\exp[2\mathrm{Re}(\theta_3)] + A_{12}\exp(\theta_1 + \theta_2^\star) + A_{13}\exp(\theta_1 + \theta_3^\star) \\ & + A_{23}\exp(\theta_2 + \theta_3^\star) + A_{12}^\star\exp(\theta_1^\star + \theta_2) + A_{13}^\star\exp(\theta_1^\star + \theta_3) + A_{23}^\star\exp(\theta_2^\star + \theta_3) + D_{1212}\exp[2\mathrm{Re}(\theta_1) + 2\mathrm{Re}(\theta_2)] \\ & + D_{1313}\exp[2\mathrm{Re}(\theta_1) + 2\mathrm{Re}(\theta_3)] + D_{2323}\exp[2\mathrm{Re}(\theta_2) + 2\mathrm{Re}(\theta_3)] + D_{1312}\exp[2\mathrm{Re}(\theta_1) + \theta_3 + \theta_2^\star] \\ & + D_{1213}\exp[2\mathrm{Re}(\theta_1) + \theta_2 + \theta_3^\star] + D_{2312}\exp[2\mathrm{Re}(\theta_2) + \theta_3 + \theta_1^\star] + D_{1223}\exp[2\mathrm{Re}(\theta_2) + \theta_1 + \theta_3^\star] \\ & + D_{2313}\exp[2\mathrm{Re}(\theta_3) + \theta_2 + \theta_1^\star] + D_{1323}\exp[2\mathrm{Re}(\theta_3) + \theta_1 + \theta_2^\star] + q_{123123}\exp[2\mathrm{Re}(\theta_1) + 2\mathrm{Re}(\theta_2) + \mathrm{Re}(\theta_3)], \end{aligned} \tag{B10b}$$

where

$$A_{ij} = 1/4(\omega_i + \omega_i^\star)^2, \quad (i,j = 1,2,3), \tag{B11a}$$

$$C_{121} = 4A_{11}A_{12}^\star(\omega_2 - \omega_1)^2, \quad C_{131} = 4A_{11}A_{13}^\star(\omega_3 - \omega_1)^2, \quad C_{122} = 4A_{22}A_{12}^\star(\omega_2 - \omega_1)^2, \tag{B11b}$$

$$C_{232} = 4A_{22}A_{23}^{\star}(\omega_3-\omega_2)^2, \quad C_{133} = 4A_{33}A_{13}(\omega_3-\omega_1)^2, \quad C_{233} = 4A_{33}A_{23}(\omega_3-\omega_2)^2, \tag{B11c}$$

$$C_{231} = 4A_{13}A_{12}^{\star}(\omega_3-\omega_2)^2, \quad C_{132} = 4A_{12}A_{23}^{\star}(\omega_3-\omega_1)^2, \quad C_{123} = 4A_{13}A_{23}(\omega_2-\omega_1)^2, \tag{B11d}$$

$$D_{1212} = A_{22}|C_{121}|^2/A_{11}, \quad D_{1313} = A_{33}|C_{131}|^2/A_{11}, \quad D_{2323} = A_{33}|C_{232}|^2/A_{22}, \quad D_{1312} = A_{23}^{\star}C_{121}^{\star}C_{131}/A_{11}, \tag{B11e}$$

$$D_{2312} = A_{13}^{\star}C_{122}^{\star}C_{232}/A_{22}, \quad D_{2313} = A_{12}^{\star}C_{133}^{\star}C_{233}/A_{33}, \quad D_{1213} = D_{1312}^{\star}, \quad D_{1223} = D_{2312}^{\star}, \quad D_{1323} = D_{2313}^{\star}, \tag{B11f}$$

$$F_{12312} = 4D_{1212}D_{1312}(\omega_3-\omega_2)^2/C_{121}^{\star}, \quad F_{12313} = 4D_{1313}D_{2313}(\omega_2-\omega_1)^2/C_{133}^{\star}, \tag{B11g}$$

$$F_{12323} = 4D_{2323}D_{1223}(\omega_3-\omega_1)^2/C_{232}^{\star}, \quad q_{123123} = A_{11}|F_{12323}|^2/D_{2323}, \tag{B11h}$$

with $\omega_m = \omega_m\bar{t} - \kappa_m y + \theta_{0m}$, $(m = 1,2,3)$, θ_{0m} standing for arbitrary constants. The dispersion equation is given by $\omega_m\kappa_m + 1 = 0$, and the wave constants are expressed by Eqs. (B8) and (B9).

[1] T. Brabec and F. Krauz, Rev. Mod. Phys. **72**, 545 (2000); N. Karasawa, S. Nakamura, N. Nakagawa, M. Shibata, R. Morita, H. Shigekawa, and M. Yamashita, IEEE J. Quantum Electron. **37**, 398 (2001).

[2] Y. S. Kivshar and G. P. Agrawal, *Optical Solitons: From Fibers to Photonic Crystals* (Academic, New York, 2003).

[3] G. P. Agrawal, *Nonlinear Fiber Optics* (Academic Press, New York, 1994); Y. R. Shen, *The Principles of Nonlinear Optics* (John Wiley & Sons, New York, 1984); R. W. Boyd, *Nonlinear Optics* (Academic Press, New York, 1994); A. Yariv, *Quantum Electronics* (John Wiley & Sons, New York, 1989); H. A. Haus, *Waves and Fields in Optoelectronics* (Prentice-Hall, Englewood Cliffs, NJ, 1984); A. E. Siegman, *Lasers* (University Science Books,Mill Valley, CA, 1986); J.-C. Diels and W. Rudolph, *Ultrashort Laser Pulse Phenomena* (Academic Press, New York, 1996); K. J. Blow and D. Wood, IEEE J. Quant. Electron. **25**, 2665 (1989); R. M. Joseph *et al.*, Opt. Lett. **18**, 491 (1993); R. W. Ziolkowski and J. B. Judkins, J. Opt. Soc. Am. B **10**, 186 (1993); C. V. Hile and W. L. Kath, *ibid.* **13**, 1135 (1996); R. G. Flesch, A. Pushkarev, and J. V. Moloney, Phys. Rev. Lett. **76**, 2488 (1996); V. G. Bespalov, S. A. Kozlov, Yu. A. Shpolyansky, and I. A. Walmsley, Phys. Rev. A **66**, 013811 (2002); S. A. Skobelev, D. V. Kartashov, and A. V. Kim, Phys. Rev. Lett. **99**, 203902 (2007); A. V. Kim and S. A. Skobelev, Phys. Rev. A **83**, 063832 (2011); A. V. Kim, S. A. Skobelev, D. Anderson, T. Hansson, and M. Lisak, *ibid.* **77**, 043823 (2008); A. A. Drozdov, S. A. Kozlov, A. A. Sukhorukov, and Yu. S. Kivshar, *ibid.* **86**, 053822 (2012); A. N. Berkovsky, S. A. Kozlov, and Yu. A. Shpolyanskiy, *ibid.* **72**, 043821 (2005).

[4] H. G. Winful, Opt. Lett. **11**, 33 (1986).

[5] Y. Silberberg, Nature (London) **430**, 624 (2004).

[6] J. Itatani, D. Zeiller, J. Levesque, M. Spanner, D. M. Villeneuve, and P. B. Corkum, Phys. Rev. Lett. **94**, 123902 (2005).

[7] D. V. Kartashov, A. V. Kim, and S. A. Skobelev, Radiophys. Quantum Electron. **46**, 374 (2003).

[8] D. V. Kartashov, A. V. Kim, and S. A. Skobelev, JETP Lett. **78**, 276 (2003); S. A. Skobelev and A. V. Kim, *ibid.* **80**, 623 (2004).

[9] I. H. Maliton, J. Opt. Soc. Am. **55**, 1205 (1965).

[10] T. Schäfer and C. E. Wayne, Physica D **196**, 90 (2004).

[11] S. A. Kozlov, Opt. Spectrosc. **84**, 887 (1998).

[12] A. O. Ukrainsky and S. A. Kozlov, J. Opt. B **3**, 180 (2001).

[13] S. A. Kozlov and S. V. Sazonov, JETP **84**, 221 (1997).

[14] A. N. Azarenkov, G. B. Altshuler, N. R. Belashenkov, and S. A. Kozlov, Quantum Electron. **23**, 633 (1993); T. Brabec and F. Kraucz, Phys. Rev. Lett. **78**, 3282 (1997).

[15] A. A. Zabolotskii, Phys. Rev. A **85**, 063833 (2012).

[16] J. M. Burgers, *A Mathematical Model Illustrating the Theory of Turbulence*, Advances in Applied Mechanics, edited by Richard von Mises and Theodore von Kármán (Academic Press, New York, 1948), pp. 171–199.

[17] R. Hirota, *The Direct Method in Soliton Theory* (Cambridge University Press, Cambridge, 2004); Phys. Rev. Lett. **27**, 1192 (1971).

[18] H. Kedia, I. Bialynicki-Birula, D. Peralta-Salas, and W. T. M. Irvine, Phys. Rev. Lett. **111**, 150404 (2013).

[19] S. V. Sazonov and N. V. Ustinov, JETP Lett. **99**, 503 (2014).

[20] A. Sakovich and S. Sakovich, J. Phys. Soc. Jpn. **74**, 239 (2005); E. J. Parkes, Chaos Solitons Fractals **38**, 154 (2008); V. K. Kuetche, T. B. Bouetou, and T. C. Kofane, J. Phys. Soc. Jpn. **76**, 024004 (2007); Y. Matsuno, *ibid.* **76**, 084003 (2007); Phys. Lett. A **359**, 451 (2006); J. Math. Phys. **49**, 073508 (2008); S. Stalinand and M. Senthilvelan, Phys. Scr. **86**, 015006 (2012); A. J. Morrison and E. J. Parkes, Chaos Solitons Fractals **16**, 13 (2003).

[21] A. Baltuska, Z. Wei, M. S. Pshenichnikov, and D. A. Wiersma, Opt. Lett. **22**, 102 (1997); M. Nisoli *et al.*, *ibid.* **22**, 522 (1997).

[22] V. K. Kuetche, T. B. Bouetou, and T. C. Kofane, J. Phys. Soc. Jpn. **76**, 073001 (2007).

[23] Y. Matsuno, J. Math. Phys. **52**, 123702 (2011).

[24] K. Yamane, Z. Yang, Y. Toda, and R. Morita, New J. Phys. **16**, 053020 (2014).

[25] P. Sprangle and B. Hafizi, Phys. Plasmas **21**, 055402 (2014); F. Quéré *et al.*, J. Phys. B **47**, 124004 (2014).

[26] M. Wegener, *Extreme Nonlinear Optics* (Springer-Verlag, Berlin, 2005).

[27] V. N. Serkin and T. L. Belyaeva, JETP Lett. **74**, 573 (2001); V. N. Serkin and A. Hasegawa, IEEE Sel. Top. J. Quantum Electron. **8**, 418 (2002); JETP Lett. **72**, 89 (2000); Phys. Rev. Lett. **85**, 4502 (2000); T. L. Belyaeva and V. N. Serkin, in *Hydrodynamics - Advanced Topics*, edited by H. Schulz (InTech, Mexico, 2011), Chap. 3; V. N. Serkin, A. Hasegawa, and T. L. Belyaeva, J. Mod. Opt. **57**, 1456 (2010); Phys. Rev. Lett. **98**, 074102 (2007); V. K. Kuetche, T. B. Bouetou, and T. C. Kofane, in *Handbook of Solitons: Research, Technology and Applications*, edited by S. P. Lang and S. H. Bedore (Nova Science Publishers, Inc., New York, 2009), p. 854.

[28] A. Hasegawa, *Massive WDM and TDM Soliton Transmission* (Kluwer Academic, Dordrecht, 2000); J. R. Taylor, *Optical Solitons-Theory and Experiment* (Cambridge University Press, Cambridge, 1992); N. N. Akhmediev and A. Ankiewicz, *Solitons: Nonlinear Pulses and Beams* (Chapman and Hall, London, 1997); J. M. Dudley and J. R. Taylor, *Optical Fiber Supercontinuum Generation* (Cambridge University Press, Cambridge, 2010).